

1 This article was published Biofouling, 30, 535-546, 2014  
2 <http://dx.doi.org/10.1080/08927014.2014.890713>

3

4

## 5 **96-well microtiter plates for biofouling simulation in biomedical settings**

6

7 **LC Gomes<sup>1</sup>, JMR Moreira<sup>1</sup>, JS Teodósio<sup>1</sup>, JDP Araújo<sup>2</sup>, JM Miranda<sup>2</sup>, M Simões<sup>1</sup>, LF Melo<sup>1</sup>, FJ**  
8 **Mergulhão<sup>1</sup>**

9 1 LEPABE – Department of Chemical Engineering, Faculty of Engineering, University of Porto, Rua Dr.  
10 Roberto Frias, Porto, Portugal

11 2 CEFT – Department of Chemical Engineering, Faculty of Engineering, University of Porto, Rua Dr.  
12 Roberto Frias, Porto, Portugal

13

14

15

16

17

18 Corresponding author: Filipe J. M. Mergulhão, Department of Chemical Engineering, Faculty of  
19 Engineering University of Porto, Rua Dr. Roberto Frias, 4200-465 Porto, Portugal. Phone: (+351)  
20 225081668. Fax: (+351) 5081449. E-mail: [filipem@fe.up.pt](mailto:filipem@fe.up.pt).

21

22

23 WORD COUNT

24 Text: 5802 words

25 References: 2062 words

26 Figures: 583 words

27 Tables: 12 words

28 TOTAL: 6397 words

29 **Abstract**

30 Microtiter plates with 96 wells are routinely used in biofilm research mainly because they  
31 enable high-throughput assays. These platforms are used in a variety of conditions  
32 ranging from static to dynamic operation using different shaking frequencies and orbital  
33 diameters. The main goals of this work were to assess the influence of nutrient  
34 concentration and flow conditions on *Escherichia coli* biofilm formation in microtiter  
35 plates and to define the operational conditions to be used in order to simulate relevant  
36 biomedical scenarios. Assays were performed in static mode and in incubators with  
37 distinct orbital diameters using different concentrations of glucose, peptone and yeast  
38 extract. Computational fluid dynamics (CFD) was used to simulate the flow inside the  
39 wells for shaking frequencies ranging from 50 to 200 rpm and orbital diameters from 25  
40 to 100 mm. Higher glucose concentrations enhanced *E. coli* adhesion in the first 24 hours,  
41 but variation of peptone and yeast extract concentration had no significant impact on  
42 biofilm formation. Numerical simulations indicate that 96-well microtiter plates can be  
43 used to simulate a variety of biomedical scenarios if the operating conditions are carefully  
44 set.

45

46 **Keywords:** Biofilm, *Escherichia coli*, microtiter plate, nutrient concentration,  
47 computational fluid dynamics, shear strain rate

48

49 **Introduction**

50 Biofilms are responsible for many persistent and chronic bacterial infections in humans  
51 (Hancock et al. 2007). Virtually all medical implants are prone to colonization by bacteria  
52 and these biofilms often serve as a source of recurrent infections (Hancock et al. 2007).  
53 About 60-70% of the hospital acquired infections are associated with some type of

54 implanted medical device (Bryers 2008) and urinary catheter infection is the most  
55 common implant-related infection (Weinstein & Darouiche 2001). Pathogenic strains of  
56 the Gram-negative bacterium *Escherichia coli* are responsible for 70 to 95% of urinary  
57 tract infections (UTI), notably in catheterized patients (Dorel et al. 2006, Jacobsen et al.  
58 2008). In fact, more than 30 million urinary catheters are inserted per year in the United  
59 States alone and the infection rate is between 10-30% (Schinabeck & Ghannoum 2006).  
60 The annual cost of caring for patients with catheter-associated UTIs is around \$2 billion  
61 (Foxman 2002).

62 Biofilm establishment and development are dynamic and complex processes regulated by  
63 intrinsic biological properties and also by many environmental conditions (Donlan 2002).

64 It is known that hydrodynamics influence biofilm formation (Liu & Tay 2002, Stoodley  
65 et al. 2001, Wäsche et al. 2002), not only in terms of nutrient and oxygen supply (Moreira  
66 et al. 2013a), but also by the shear forces, which can modulate microbial cell adhesion to  
67 a given surface (Busscher & van der Mei 2006, Simões et al. 2007, Teodósio et al. 2013,  
68 van Loosdrecht et al. 1995). One of the key parameters affecting cell adhesion to a surface  
69 is the shear rate at that surface (Busscher & van der Mei 2006, Teodósio et al. 2013).

70 Table 1 lists commonly found shear strain rates in biomedical and miscellaneous settings  
71 where bacterial adhesion can occur. In medical devices, molecules and microorganisms  
72 are constantly exposed to shear conditions caused by liquid flow (Fux et al. 2004,  
73 Mukherjee et al. 2009). Urinary catheters and the human urinary tract are submitted to  
74 significant hydrodynamic shear forces (adult humans produce 1-2 liters of urine per day,  
75 which is expelled at average flow rates of 40-80 ml h<sup>-1</sup>) (Vejborg & Klemm 2008), but  
76 adherence to surfaces enables *E. coli* to resist removal by urine flow and establish  
77 infection (Hancock et al. 2007, Ulett et al. 2007). Besides the hydrodynamic conditions,  
78 the nutrient/substrate concentration can have impact on biofilm growth, development and

79 detachment behavior (Rochex & Lebeault 2007, Stoodley et al. 2001, Telgmann et al.  
80 2004).

81 Microtiter plates are often used for biofilm studies because small media volumes are  
82 needed (Coenye & Nelis 2010), replicate tests are easily prepared using multi-channel  
83 pipettors (Duetz 2007), and this closed (batch reactor-like) system lends itself to protocols  
84 where different media compositions are simultaneously tested (Coenye & Nelis 2010).

85 The main goals of this work were to assess the influence of nutrient concentration and  
86 flow conditions on *Escherichia coli* biofilm formation in 96-well microtiter plates and to  
87 verify if the hydrodynamic conditions that can be attained with these systems are similar  
88 to those normally encountered in diverse biomedical scenarios. A good comprehension  
89 of the hydrodynamics that are found in the areas where biofilms naturally occur is crucial  
90 for biofilm studies performed in laboratory-based devices. This enables the correct setting  
91 of operational conditions in the lab in order to obtain biofilms that resemble those found  
92 in natural environments.

93

## 94 **Materials and Methods**

### 95 *Numerical simulations*

96 Numerical simulations were made in Ansys Fluent CFD package (version 13.0). A  
97 cylindrical well (diameter of 6.6 mm and height of 11.7 mm) was built in Design Modeller  
98 13.0 and discretized into a grid of 18,876 hexahedral cells by Meshing 13.0. A grid  
99 independence analysis was performed and the results show that reducing the cell  
100 dimensions by half in all directions (corresponding to an 8 fold reduction of the cell  
101 volume) has a negligible effect (about 7.7%) when compared to the uncertainty associated  
102 with the biological data obtained in the experimental part of this work (see Supplementary  
103 material, Table S1). For each simulation, the volume of the liquid phase inside the well

104 was set to 200  $\mu\text{L}$  and the remaining volume was filled with gas. The properties of water  
105 and air at 30  $^{\circ}\text{C}$  were used for the liquid and gas phases, respectively (see Supplementary  
106 material, Table S2). The surface tension was set equal to the surface tension of an  
107 air/water system.

108 The volume of fluid (VOF) methodology (Hirt & Nichols 1981) was used to track the  
109 liquid/gas interface and the precise locations of the interface were obtained by the Geo-  
110 Reconstruct method (Youngs 1982). The velocity-pressure coupled equations were  
111 solved by the PISO algorithm, the QUICK scheme was used for the discretization of the  
112 momentum equations and the PRESTO! scheme was chosen for pressure discretization.

113 In Ansys Fluent, the surface tension effects were modeled by the continuum surface force  
114 (Brackbill et al. 1992), which were introduced through a source term in the momentum  
115 equation. An accelerating reference frame was adopted, and the circular orbital motion  
116 was taken into account by introducing another source term that represents the effect of  
117 the force into the fluid resulting from this orbital motion. The no slip boundary condition  
118 and a contact angle of  $83^{\circ}$  were considered for all the walls (Simões et al. 2010a).

119 Simulations were made for different shaking frequencies (50 to 200 rpm) and orbital  
120 diameters (25 to 100 mm). For each case, 5 s of physical time were simulated with a fixed  
121 time step of  $2.5 \times 10^{-4}$  s. The primary numerical results were the instantaneous velocity  
122 components, the instantaneous pressure and the liquid or gas phase volume fractions.

123 These results were used to determine the shear rate, the location of the interface and the  
124 air-liquid interfacial area. The magnitude of the shear strain rate was determined by Ansys  
125 Fluent with the help of a built-in expression. For each simulation, after the steady state is  
126 reached, the average shear strain rate was calculated by integrating an instantaneous  
127 solution over the wetted area. The time averaged shear strain rate was obtained by  
128 averaging the steady state shear rate of the liquid side during a complete orbit.

129

130 ***Bacterial strain***

131 *Escherichia coli* JM109(DE3) from Promega (USA) was used for biofilm formation. Its  
132 genotype is *endA1, recA1, gyrA96, thi, hsdR17* ( $r_k^-$ ,  $m_k^+$ ), *relA1, supE44,  $\lambda^-$ ,  $\Delta(lac-$   
133 *proAB)*, [*F'*,*traD36, proAB, lacI<sup>q</sup>Z $\Delta$ M15*],  $\lambda$ (DE3). *E. coli* CECT 434 (ATCC 25922), a  
134 clinical isolate often used for antimicrobial susceptibility tests, was also used for  
135 confirmation of the results in selected conditions. An overnight culture of *E. coli* was  
136 prepared as described by Teodósio et al. (2011b). Cells were harvested by centrifugation  
137 and appropriate dilutions in sterile saline (NaCl 0.85%) were performed to obtain an  
138 optical density (OD) of approximately 0.4 at 610 nm.*

139

140 ***Culture conditions and biofilm quantitation***

141 Different media formulations were assayed using a reference medium recipe that had  
142 already been tested for biofilm formation in a flow cell with the same strain (Teodósio et  
143 al. 2011b). This reference medium consisted of 0.5 g l<sup>-1</sup> glucose, 0.25 g l<sup>-1</sup> peptone, 0.125  
144 g l<sup>-1</sup> yeast extract and phosphate buffer (0.188 g l<sup>-1</sup> KH<sub>2</sub>PO<sub>4</sub> and 0.26 g l<sup>-1</sup> Na<sub>2</sub>HPO<sub>4</sub>), pH  
145 7.0. A glucose concentration of 0.15 g l<sup>-1</sup> was also tested in that study and it was shown  
146 that there were no significant changes in the amount of biofilm formed (Teodósio et al.  
147 2011b). On that work, when the glucose concentration was reduced to 0.15 g l<sup>-1</sup>, the  
148 peptone and yeast concentrations were also reduced to 0.07 and 0.03 g l<sup>-1</sup>, respectively.  
149 Since preliminary results (Moreira et al. 2013b) had shown that glucose concentration has  
150 a significant impact on the amount of biofilm formed in microtiter plates (concentrations  
151 of 0.25 and 1 g l<sup>-1</sup> were assayed), an intermediate concentration (0.5 g l<sup>-1</sup>) was also tested.  
152 Additionally, since it was shown that in turbulent flow conditions higher nutrient loads  
153 generally yield thicker biofilms (Teodósio et al. 2011a), the effect of increasing the

154 peptone and yeast extract concentrations independently was assessed starting from their  
155 reference values of 0.25 and 0.125 g l<sup>-1</sup>, respectively. Thus a concentration range of 0.25,  
156 0.5 and 1 g l<sup>-1</sup> was used for glucose and peptone, whereas for yeast extract concentrations  
157 of 0.125, 0.5 and 1 g l<sup>-1</sup> were tested.

158 For each formulation, the reference culture medium (Teodósio et al. 2011b) was prepared  
159 without the compound under study and then the appropriate volume of a concentrated  
160 solution of that nutrient was added to obtain the desired concentration. 96-well  
161 polystyrene microtiter plates were inoculated as described by Moreira et al. (2013b) and  
162 incubated at 30 °C in two separate orbital incubators operating at the same shaking  
163 frequency (150 rpm). One of the incubators had a 50 mm orbital shaking diameter  
164 (CERTOMAT® BS-1, Sartorius AG, Germany) and another had a 25 mm shaking  
165 diameter (AGITORB 200, Aralab, Portugal). An additional set of experiments was  
166 performed with no shaking (0 rpm) at 30 °C. This temperature was chosen because in  
167 previous works this particular *E. coli* strain was proven to be a good biofilm producer at  
168 30 °C (Teodósio et al. 2012). Biofilm formation was monitored for 60 h with plates being  
169 removed from the incubators every 12 h for biofilm quantification (for time zero the plates  
170 were not incubated at all). Three independent experiments were performed for each  
171 shaking condition. For control, quantifications were also conducted in the absence of  
172 bacteria, demonstrating that no biofilm growth occurred in the correspondent wells during  
173 the experimental time.

174 Biofilm quantitation by crystal violet (CV) assay was performed as described by Moreira  
175 et al. (2013b). The OD was measured at 570 nm using a microtiter plate reader  
176 (SpectraMax M2E, Molecular Devices) and the biofilm amount was expressed as OD<sub>570</sub>  
177 nm values. In order to confirm the results obtained by the CV method, biofilm quantitation  
178 in selected conditions was also performed using viable plate counting (see Supplementary

179 material, Figure S1), as described by Simões et al. (2005). Both methods showed good  
180 correlation ( $r^2=0.988$ ) as previously reported by Alnnasouri et al. (2011) and Sonak &  
181 Bhosle (1995).

182

### 183 ***Scanning electron microscopy (SEM)***

184 Microtiter plate wells containing biofilms were observed by SEM after 24 h of incubation  
185 using the reference medium defined by Teodósio et al. (2011b). Prior to SEM  
186 observations, biofilm samples were prepared as reported by Ganderton et al. (1992) and  
187 wall sections were cut out and sputter-coated as described by Simões et al. (2007). SEM  
188 observations were carried out using SEM/EDS (FEI Quanta 400FEG ESEM/EDAX  
189 Genesis X4M).

190

### 191 ***Calculations and statistical analysis***

192 The results presented in Figure 5 are an average of those obtained in three independent  
193 experiments for each shaking condition (50 and 25 mm orbital shaking diameter at 150  
194 rpm and no shaking). For a single experiment, the final value is an average of the readings  
195 obtained in 6 replica wells within one plate. The following standard deviations (SDs)  
196 were obtained for the glucose experiments, 34%, 22% and 27% (50 mm, 25 mm and no  
197 shaking, respectively). For peptone 36%, 25% and 22%, and for yeast extract 19%, 25%  
198 and 26% (in the same order).

199 With the aim of ascertaining the statistical significance, data was analysed using IBM  
200 SPSS Statistics software version 19.0. The parametric Post Hoc Multiple Comparisons  
201 Tests – Tukey and LSD – were used based on a confidence level of 95% (differences  
202 reported as significant for P values < 0.05). The following statistical analysis were  
203 conducted: a - comparison between 1 g l<sup>-1</sup> and 0.5 g l<sup>-1</sup> glucose or peptone or yeast extract,



204 b - comparison between 1 g l<sup>-1</sup> and 0.25 g l<sup>-1</sup> glucose or peptone, c - comparison between  
205 0.5 g l<sup>-1</sup> and 0.25 g l<sup>-1</sup> glucose or peptone, d - comparison between 0.5 g l<sup>-1</sup> and 0.125 g l<sup>-1</sup>  
206 yeast extract, e - comparison between 1 g l<sup>-1</sup> and 0.125 g l<sup>-1</sup> yeast extract (see Figure 5).  
207 Paired *t*-test analysis was also performed when appropriate.

208

## 209 **Results**

### 210 *CFD modelling of shaken 96-well microtiter plates*

211 In an orbital shaker, the inclination of the air-liquid interface increases with the increase  
212 of the shaking frequency and the orbital diameter. This effect can be quantified by  
213 measuring the angle of the surface formed with the horizontal (Figure 2A). A maximum  
214 angle of 34° was obtained for the largest orbital diameter and shaking frequency. The  
215 maximum height of the interface (*h*), normalized by the height of the well (*H<sub>w</sub>*), is  
216 represented in Figure 2B as a function of the shaking frequency for different orbital  
217 diameters. This dimensionless parameter is an indication of the volume of the well  
218 occupied by the liquid. Values ranging from 46 to 67% were obtained (with the highest  
219 values corresponding to the larger orbital diameter and shaking frequency), indicating  
220 that the liquid does not overflow from the well in any of the simulated situations. As the  
221 slope of the interface increased, the interfacial area also increased. Figure 2C shows the  
222 ratio between the specific surface area in a moving well (*a<sub>f</sub>*) and the specific surface area  
223 in a stationary well (*a<sub>i</sub>*) for several shaking frequencies and orbital amplitudes. When the  
224 *a<sub>f</sub>/a<sub>i</sub>* ratio is greater than 1, this means that an area gain is obtained with the orbital  
225 motion. The area gain was negligible (less than 2%) for the smaller orbital diameter  
226 regardless of the shaking frequency. For all the orbital diameters, area gains ranging from  
227 0.4-2% were obtained for shaking frequencies up to 150 rpm (except for 75 and 100 mm  
228 at 150 rpm where the gains were of 5 and 8%, respectively). The highest area gain (of

229 31%) was obtained for the largest orbital diameter and shaking frequency. It is also  
230 possible to observe from Figure 2C that the slope of area gain increased significantly with  
231 the orbital diameter from 150 to 200 rpm. The evolution of the wetted area ( $A_w$ )  
232 normalized by the wetted area for a stationary well ( $A_{wi}$ ) is represented on Figure 2D. It  
233 follows the same trend that was observed for the maximum height of the interface (Figure  
234 2B), representing the available area for biofilm formation. At lower shaking frequencies  
235 (50 and 100 rpm), the wetted area remained practically constant at different orbital  
236 diameters (area gains less than 5%), but for higher frequencies area gains ranging from 4  
237 to 34% were determined.

238 The increase of the amplitude of the interfacial surface oscillation led to an increase in  
239 the fluid velocity and, consequently, to an increase of the shear strain rate near the walls  
240 of the well. Figure 3 compares the time averaged wall strain rate distribution for several  
241 orbital diameters and shaking frequencies. The wall strain rate was not uniform, being  
242 much higher in the liquid side near the interface. A zone of wall strain rate above  $30\text{ s}^{-1}$   
243 was visible for all the systems shown in Figure 3, and was delimited by the region where  
244 the interface oscillates. The extension of this region increased as the shaking frequency  
245 and orbital diameter increased. For all orbital diameters, the average strain rate is around  
246  $12\text{ s}^{-1}$  when a shaking frequency of 50 rpm is used (Figure 4). However, when an  
247 incubator with 25 mm of shaking amplitude is used, this value can be increased 3 fold  
248 under a shaking frequency of 200 rpm. A wider range of shear rate conditions can be  
249 experienced with incubators of 50 or 75 mm orbital diameters, where numerical  
250 simulations predicted an increase of 6 to 7 fold at the highest tested frequency when  
251 compared to the value obtained at 50 rpm. Indeed, as the orbital diameter increased the  
252 shear strain range widened, spanning from 10 to  $142\text{ s}^{-1}$  (Figure 4).

253

254 ***Biofilm formation***

255 The combined effects of shear forces and nutrient levels on biofilm formation were  
256 assessed by crystal violet assay (Figure 5). Polystyrene 96-well microtiter plates were  
257 placed in orbital incubators with shaking diameters of 25 and 50 mm (at the same shaking  
258 frequency of 150 rpm) and also without shaking (0 rpm). Simultaneously, the influence  
259 of three concentrations of the main nutrients (glucose, peptone and yeast extract) was  
260 studied.

261 Figures 5A, B and C, concerning the effect of glucose, show that the initial biofilm  
262 production (until 12 h) was 51% higher on the lower concentration media (0.25 and 0.5 g  
263 l<sup>-1</sup>) for the highest shaking amplitude. Opposite results were observed for the lower  
264 amplitude and also for the static condition (statistically significant differences were  
265 obtained between the two extreme concentrations in all shaking conditions). For the  
266 highest glucose concentration (1 g l<sup>-1</sup>), a maximum in biofilm formation was attained at  
267 24 h in all shaking conditions. Above 24 h, whilst the biofilm amount decreased from the  
268 maximum in both shaking conditions (in particular for the higher shaking amplitude), this  
269 maximum amount was relatively the same on the static condition. Interestingly,  
270 approximately the same maximum amount of biofilm was formed in all hydrodynamic  
271 conditions ( $P = 0.41$ ) for the highest glucose concentration tested.

272 When analysing the oscillatory behavior in detail for the highest shaking amplitude  
273 (Figure 5A), it is possible to see that the decrease in the biofilm amount in the culture  
274 medium with 1 g l<sup>-1</sup> glucose was abrupt between 24 and 36 h, reaching the level obtained  
275 with the intermediate glucose concentration at the end of the experiment (60 h). For 0.5  
276 g l<sup>-1</sup> glucose, the fluctuations were also observed (the maximum was reached at 36 h),  
277 nevertheless with a smoother decrease than the one found for the most concentrated  
278 medium.

279 When an orbital shaker with 25 mm diameter at 150 rpm was used (Figure 5B), the  
280 general trend is that the amount of biofilm formed increased with increasing glucose  
281 concentrations. For this hydrodynamic condition and with 1 g l<sup>-1</sup> glucose, the decrease of  
282 biofilm amount between 24 and 36 h was less pronounced than in the larger diameter  
283 incubator (35% versus 74% decrease, respectively). Then, the amount of biofilm  
284 stabilized until the end of the experiment, and similar values to those obtained with the  
285 larger shaking diameter were achieved ( $P = 0.45$ ).

286 Concerning the effect of peptone concentrations (Figures 5D, E and F), the maximum  
287 biofilm amount was obtained at 36 h ( $P < 0.05$ ) for the highest concentration (1 g l<sup>-1</sup>) and  
288 shaking diameter (Figure 5D). From this moment onwards, the amount of biofilm  
289 obtained with this growth medium markedly decreased (80%) to the final level of the  
290 remaining media. Except for this maximum value, the differences found when varying  
291 peptone concentrations were not statistically significant for the majority of the time points  
292 in both agitated conditions (Figures 5D and E). For the static condition (Figure 5F), it can  
293 be seen that increasing the concentration of this compound promoted biofilm growth in  
294 the early stages of biofilm development.

295 Figures 5G, H and I show the effect of yeast extract concentrations on biofilm formation  
296 under the tested hydrodynamic conditions. In terms of statistical significance, the results  
297 indicate that this is the nutrient for which less significant differences were obtained under  
298 the experimented concentrations (0.125, 0.25 and 1 g l<sup>-1</sup>). Comparing the results for each  
299 concentration of yeast extract between both orbital shaking diameters, the growth profiles  
300 were very similar ( $P > 0.05$  for 87% of time points), showing that the orbital shaking  
301 diameter had negligible impact on *E. coli* biofilm formation when different levels of yeast  
302 extract were used.

303 Figure 6 shows the biofilm distribution on the vertical wall of 96-well microplates.  
304 Biofilms consisting of cell clumps (Figure 6A) were observed in the liquid side near the  
305 interface where, according to the CFD modeling, cells are exposed to higher magnitudes  
306 of shear strain rate (Figure 3). Outside this wall region, the biofilm cell density decreased  
307 and *E. coli* single cells were homogeneously distributed on the surface (Figure 6B). A  
308 similar cell pattern was observed for the static condition albeit with a lower cell density  
309 (Figure 6C).

310

## 311 **Discussion**

### 312 *CFD modelling of shaken 96-well microtiter plates*

313 Because hydrodynamics have such a great impact on biofilm formation in terms of  
314 nutrient and oxygen transfer, and also influence cell attachment to and removal from  
315 surfaces (Simões et al. 2007, Stoodley et al. 1998, Teodósio et al. 2013), it is interesting  
316 to estimate by CFD several hydrodynamic parameters such as the average strain rate, the  
317 specific air-liquid surface area and the wetted area available for cell adhesion.

318 As previously suggested by Hermann et al. (2003) and Kensy et al. (2005), the angle of  
319 the liquid surface in the wells increases exponentially with increasing shaking intensities  
320 (shaking diameters and shaking frequencies at constant filling volume), and an  
321 enlargement of the specific air-liquid mass transfer area ( $a_f/a_i$ ) is obtained. The  
322 numerical results also show that, at lower shaking frequency and especially for the lowest  
323 shaking amplitude tested, the surface tension force dominates and keeps the liquid surface  
324 nearly in the horizontal state. This corroborates the experimental results obtained by  
325 Ortiz-Ochoa et al. (2005) and Hermann et al. (2003). Images acquired with a CCD-camera  
326 for wells filled with 200  $\mu$ l water and shaken at a shaking diameter of 25 mm showed no  
327 liquid movement below 200 rpm (Hermann et al. 2003). In this study, a change of the

328 hydrodynamic flow is visible above 100 rpm (approximately the critical shaking  
329 frequency) when the increased centrifugal force starts to gain relevance when compared  
330 to surface tension. With a further increase of shaking frequency, the maximum liquid  
331 height also increases and an expansion of the air-liquid mass transfer area is obtained  
332 (Hermann et al. 2003), providing better oxygen transfer to the liquid. From these results,  
333 it is reasonable to conclude that the surface tension has a strong influence on the  
334 hydrodynamic flow and likely on the mass transfer in 96-well microtiter plates.

335 The experimental shaking conditions chosen for this work ( $d_o = 25$  and  $50$  mm,  $150$  rpm)  
336 can reproduce the hydrodynamics of urinary catheters where *E. coli* typically adheres.  
337 The shear strain rate found on these devices is of approximately  $15\text{ s}^{-1}$  (Bakker et al. 2003,  
338 Velraeds et al. 1998), which is only slightly lower than the range obtained under the  
339 experimented conditions, according to the numerical results ( $23\text{-}46\text{ s}^{-1}$ ). With the shaking  
340 amplitudes and frequencies used for biofilm formation in microtiter plates, it is also  
341 possible to attain the shear strain rates that are found in the oral cavity, arteries and veins  
342 (Table 1). For instance, the shear strain rate in the oral cavity can be simulated with the  
343 same incubators shaking at frequencies up to  $150$  rpm. In order to reproduce the shear  
344 rates resulting from the blood flow in arteries, it is vital to work with larger orbital  
345 diameters ( $75$  or  $100$  mm) at shaking frequencies around  $100$  rpm or with shaking  
346 frequencies above the simulated ones for all shaking amplitudes. In this latter case, one  
347 must bear in mind that a splashing phenomenon can occur for larger diameters and  
348 frequencies above  $200$  rpm. This is not experimentally feasible due to contamination and  
349 loss of growth medium and cells. Regarding the non-biomedical scenarios, it is possible  
350 to attain the same shear rates encountered on a ship hull in a harbor with the  $50$  mm  
351 incubator at  $150$  rpm or with the other incubators of larger diameter at velocities around

352 100 rpm. Finally, the liquid flow in biofilm channels should be simulated under the  
353 shaking conditions already indicated for the blood flow in arteries.

354 Possible improvements of the system described in this work may come from the use of  
355 orbital shakers with larger shaking amplitudes (eg 75 or 100 mm) at the same frequency  
356 (150 rpm). In these incubators there is a higher gain in the wetted area and the air-liquid  
357 interface area during shaking, which possibly results in relatively high specific oxygen  
358 transfer rates and further increase in microbial growth (Duetz 2007, Duetz et al. 2000).

359 Although microtiter plates have been extensively used for biofilm studies in the last years  
360 (Castelijjn et al. 2012, Leroy et al. 2007, Rodrigues & Elimelech 2009, Shakeri et al.  
361 2007), little is known about the flow pattern inside the wells. In fact, few papers have  
362 been published applying computational fluid dynamics to simulate flow in microtiter  
363 plates (Barrett et al. 2010, Zhang et al. 2008) during biofilm formation. Azevedo et al.  
364 (2006) simulated the flow inside 6-well plates to test the influence of shear stress,  
365 temperature and inoculation concentration on the adhesion of *Helicobacter pylori* to  
366 stainless steel and polypropylene coupons. Kostenko et al. (2010) studied *Staphylococcus*  
367 *aureus* deposition in the same plate format using different filling volumes and agitation  
368 frequencies. This latter system was further analyzed by CFD by Salek et al. (2012) using  
369 a flow topology analysis to explain biofilm accumulation, morphology and orientation of  
370 endothelial cells. Since the 96-well format is currently one of the favorite platforms for  
371 biofilm studies, it is intriguing why such a lack of information exists for this system. Our  
372 research group started to study its hydrodynamics by monitoring the influence of two  
373 shaking conditions on *E. coli* biofilm development (Moreira et al. 2013b). This simulation  
374 was now extended in order to define which operational conditions should be chosen for  
375 each particular application. When trying to produce “artificial” biofilms in laboratory  
376 reactors one has to make sure that these biofilms resemble those that are formed in natural

377 environments. If that is not the case, then important experiments regarding antibiotic  
378 susceptibilities, resistance to mechanical treatment, biocide efficacy assays and other tests  
379 will not produce reliable results that are indeed applicable to the “natural” biofilms that  
380 need to be controlled (Buckingham-Meyer et al. 2007). Since some knowledge about the  
381 hydrodynamics of the locations where “natural” biofilms form is already available, it is  
382 important that laboratory experiments are carried out in a way that mimics those  
383 conditions. The information presented on this work defines the applicability range of 96-  
384 well microtiter plates in the simulation of several natural scenarios where biofilms form.

385

### 386 ***Biofilm formation***

387 In this work, the effects of glucose, peptone and yeast extract concentrations on biofilm  
388 development were tested. The reference concentration of each nutrient that was used on  
389 the previous study (Teodósio et al. 2011b) and higher concentrations of the three main  
390 nutrients were tested because it has been reported that high nutrient concentrations can  
391 favor biofilm formation (Frias et al. 2001, Klahre & Flemming 2000, Volk &  
392 LeChevallier 1999).

393 In preliminary studies, the effect of incubation temperature on biofilm formation was  
394 studied in selected conditions. A wide range of medical devices are currently used  
395 including indwelling (Donlan 2001), partially implantable and external devices (Newman  
396 2008). A temperature of 37 °C is more appropriate for simulating indwelling devices in  
397 body core sites and temperatures closer to 25 °C are best suited for external devices.  
398 Therefore, an average temperature of 30 °C is a good approximation for a partially  
399 implantable device in body peripheral/skin sites (Andersen et al. 2010). Experiments  
400 assaying the effect of temperature have shown that biofilm formation at 30 °C is usually  
401 favored when compared to 37 °C for the tested conditions, but the results obtained are not



402 statistically different (data not shown). The influence of temperature on the  
403 hydrodynamics was also investigated. CFD simulations shown that it is negligible and  
404 even when the average strain rates are compared at the two temperatures (see  
405 Supplementary material, Figure S2), the differences are on average below 5% (for the  
406 150 rpm case used in the experimental part of this work, the difference is 0.4%). Since  
407 microtiter plate assays are often used to screen compounds for antimicrobial activity  
408 (Shakeri et al. 2007) and biofilm formation seems to be promoted at 30 °C, this  
409 temperature was chosen as an average for simulating conditions found in indwelling,  
410 external and partially implantable devices.

411 The overall results of the glucose experiments indicate that higher glucose concentrations  
412 may be beneficial for *E. coli* adhesion in the first 24 hours, independently of the shaking  
413 conditions. Despite the lack of information on *E. coli* biofilms, it has been reported  
414 (Bühler et al. 1998) that the total yield of cells growing in a biofilm increased linearly  
415 with increase of glucose up to 2 g l<sup>-1</sup>. For *Pseudomonas* species, independent groups noted  
416 that an increase in nutrient concentration is associated with an increase of cell attachment  
417 (Peyton 1996, Simões et al. 2010b). For *Pseudomonas putida*, Rochex and Lebeault  
418 (2007) observed an increase in biofilm thickness when increasing glucose concentration  
419 up to a certain limit (0.5 g.l<sup>-1</sup>), above which an additional increase of substrate reduced  
420 the biofilm accumulation rate as a consequence of a higher detachment.

421 In most cases *E. coli* cells took more time to establish on the surface under static  
422 conditions. On the other hand, after the initial period of adhesion, the amount of biofilm  
423 formed under static conditions remained constant while that accumulated under shaking  
424 conditions dropped, in particular for the glucose experiments. This corroborates what has  
425 been postulated by several authors (Percival et al. 1999, Pereira & Vieira 2001, Vieira et  
426 al. 1993), that higher flow rates can cause two phenomena of opposite nature: on the one

427 hand, they favor the transport of nutrients to the surface, contributing to cell growth in  
428 the microbial layer and to the production of exopolymers and, on the other hand, with  
429 increasing flow velocity the shear rates increase and that can cause further erosion and  
430 detachment of biofilm portions, and the consequent decrease in the amount of biomass  
431 attached to the surface. The interplay between these two effects (including the increase in  
432 surface area available for oxygenation) explains the higher growth followed by the more  
433 abrupt drop in biomass when the highest glucose concentration was used. Besides that, it  
434 is also known that *E. coli*, under certain conditions, adheres more strongly to surfaces  
435 with increasing fluid velocities due to the action of the lectin-like adhesin FimH (Thomas  
436 et al. 2002) or of the flagella (McClaine & Ford 2002).

437 Biofilms seemed to have entered a state of dynamic equilibrium at the highest shaking  
438 amplitude and for the two highest concentrations of glucose, probably as a consequence  
439 of the combined effects of hydrodynamics and carbon levels. The cyclical biofilm  
440 maturation and subsequent dispersal pattern probably occurred because it was no longer  
441 profitable for the bacterium to participate in the biofilm, due to several reasons such as  
442 shear forces, lack of nutrients and accumulation of toxic metabolic by-products (Dunne  
443 2002).

444 The data presented in this work indicates that variation of peptone and yeast extract  
445 concentrations has no significant impact on the amount of attached cells, in the range of  
446 concentrations and hydrodynamic conditions tested. As glucose is the main carbon source  
447 in the tested culture media, peptone is the most important nitrogen source since its  
448 nitrogen content exceeds 13% (Merck, product information ref. 107214). Yeast extract  
449 also provides nitrogen (> 10 %) to bacteria besides vitamins, amino acids and carbon  
450 (Merck, product information, ref. 103753). In reactors for biological waste gas treatment,  
451 biofilm growth seems to respond strongly to the amount of available nitrogen (Holubar

452 et al. 1999). A similar behavior was observed for *P. putida* strain isolated from a paper  
453 machine (Rochex & Lebeault 2007). The rate and extent of biofilm accumulation  
454 increased with nitrogen concentration (from carbon/nitrogen = 90 to carbon/nitrogen =  
455 20). Additionally, it is known that when the carbon/nitrogen ratio on the nutrient supply  
456 is increased, the polysaccharide/protein ratio generally increases (Huang et al. 1994).  
457 Delaquis et al. (1989) showed that the depletion of nitrogen led to the active detachment  
458 of cells from *P. fluorescens* biofilm. Since different *E. coli* strains are capable of causing  
459 UTI (Salo et al. 2009), selected experiments were performed to see if the results obtained  
460 with strain JM109(DE3) were also confirmed with another strain. *E. coli* CECT 434 (a  
461 clinical isolate) was used for this purpose and in general there were no statistically  
462 significant differences between the results obtained for the two strains (see  
463 Supplementary material, Figure S3).

464 Although the wetted area predicted for cell adhesion was 2 fold higher for the 50 mm  
465 incubator when compared to the 25 mm incubator (at 150 rpm), the maximum biofilm  
466 amount detected by the crystal violet assay was very similar for the three operational  
467 conditions used. Thus, an increase in wetted area did not cause an increase in the amount  
468 of biofilm.

469 The simulation results indicate that the strain rates under which the *E. coli* biofilms  
470 develop changed drastically along the cylindrical wall. The higher strain rates below the  
471 interface were associated with the formation of dispersed cell aggregates, while a decrease  
472 in the strain rate values resulted in a homogeneous distribution of single cells on the wall.  
473 Kostenko et al. (2010) also shown that biofilm deposition and morphology in microtiter  
474 plates is non-uniform and that the biofilm characteristics correlate strongly with local  
475 shear stress mean and fluctuation levels. It has been shown that biofilms in the human  
476 body are naturally heterogeneous as a result of the shear stress variations. Thus, microtiter

477 plates are ideally suited to mimic these natural variations in the shear stress field in  
478 biomedical scenarios.

479 Taking together the results obtained from the numerical simulation and those obtained  
480 during biofilm formation studies, it is possible to conclude that if the right operational  
481 conditions are used, the microtiter plate is a powerful platform for biofilm simulation in  
482 a variety of applications including biomedical scenarios.

483

#### 484 **Acknowledgments**

485 The authors acknowledge the financial support provided by Operational Programme for  
486 Competitiveness Factors – COMPETE, European Fund for Regional Development –  
487 FEDER and by the Portuguese Foundation for Science and Technology – FCT, through  
488 Projects PTDC/EQU-FTT/105535/2008 and PTDC/EBB-BIO/104940/2008. Luciana  
489 Gomes acknowledges the receipt of a Ph.D. grant from FCT (SFRH/BD/80400/2011) and  
490 José Araújo acknowledges the financial support from FCT through the Grant  
491 SFRH/BPD/64148/2009.

492

#### 493 **Nomenclature**

494  $a_f$  Final specific surface area ( $\text{m}^{-1}$ )  
495  $a_i$  Initial specific surface area ( $\text{m}^{-1}$ )  
496  $A_w$  Wetted area ( $\text{m}^2$ )  
497  $A_{wi}$  Wetted area for a stationary well ( $\text{m}^2$ )  
498  $d_o$  Shaking diameter (m)  
499  $D$  Well or vessel diameter (m)  
500  $h$  Maximum height of the interface (m)  
501  $H$  Well height (m)

502  $\theta$  Surface angle (°)

503

504 **References**

505 Aleviadrou BR, McIntire LV. 1995. Rheology. In: Loscalzo J, Schafer A, editors.  
506 Thrombosis and hemorrhage. Cambridge (MA): Blackwell Sciences; p. 369–384.

507 Alnnasouri M, Dagot C, Pons M-N. 2011. Comparison of four methods to assess biofilm  
508 development. Water Sci Technol. 63(3):432-439.

509 Andersen TE, Kingshott P, Palarasah Y, Benter M, Alei M, Kolmos HJ. 2010. A flow  
510 chamber assay for quantitative evaluation of bacterial surface colonization used to  
511 investigate the influence of temperature and surface hydrophilicity on the biofilm forming  
512 capacity of uropathogenic *Escherichia coli*. J Microbiol Methods. 81(2):135-140.

513 Azevedo NF, Pinto AR, Reis NM, Vieira MJ, Keevil CW. 2006. Shear stress,  
514 temperature, and inoculation concentration influence the adhesion of water-stressed  
515 *Helicobacter pylori* to stainless steel 304 and polypropylene. Appl Environ Microbiol.  
516 72(4):2936-2941.

517 Bakker D, van der Plaats A, Verkerke G, Busscher H, van der Mei H. 2003. Comparison  
518 of velocity profiles for different flow chamber designs used in studies of microbial  
519 adhesion to surfaces. Appl Environ Microbiol. 69(10):6280-6287.

520 Bark DL, Para AN, Ku DN. 2012. Correlation of thrombosis growth rate to pathological  
521 wall shear rate during platelet accumulation. Biotechnol Bioeng. 109:2642-2650.

522 Barrett TA, Wu A, Zhang H, Levy MS, Lye GJ. 2010. Microwell engineering  
523 characterization for mammalian cell culture process development. Biotechnol Bioeng.  
524 105(2):260-275.

525 Brackbill JU, Kothe DB, Zemach C. 1992. A continuum method for modeling surface  
526 tension. J Comput Phys. 100(2):335-354.

527 Bryers JD. 2008. Medical biofilms. *Biotechnol Bioeng.* 100(1):1-18.

528 Buckingham-Meyer K, Goeres DM, Hamilton MA. 2007. Comparative evaluation of  
529 biofilm disinfectant efficacy tests. *J Microbiol Methods.* 70(2):236-244.

530 Bühler T, Ballesteros S, Desai M, Brown MRW. 1998. Generation of a reproducible  
531 nutrient-depleted biofilm of *Escherichia coli* and *Burkholderia cepacia*. *J Appl*  
532 *Microbiol.* 85(3):457-462.

533 Busscher HJ, van der Mei HC. 2006. Microbial adhesion in flow displacement systems.  
534 *Clin Microbiol Rev.* 19(1):127-141.

535 Castelijns GAA, van der Veen S, Zwietering MH, Moezelaar R, Abee T. 2012. Diversity  
536 in biofilm formation and production of curli fimbriae and cellulose of *Salmonella*  
537 *Typhimurium* strains of different origin in high and low nutrient medium. *Biofouling.*  
538 28(1):51-63.

539 Chesterton AKS, Moggridge GD, Sadd PA, Wilson DI. 2011. Modelling of shear rate  
540 distribution in two planetary mixtures for studying development of cake batter structure.  
541 *J Food Eng.* 105(2):343-350.

542 Coenye T, Nelis HJ. 2010. *In vitro* and *in vivo* model systems to study microbial biofilm  
543 formation. *J Microbiol Methods.* 83(2):89-105.

544 Delaquis PJ, Caldwell DE, Lawrence JR, McCurdy AR. 1989. Detachment of  
545 *Pseudomonas fluorescens* from biofilms on glass surfaces in response to nutrient stress.  
546 *Microbial Ecol.* 18(3):199-210.

547 Donlan RM. 2001. Biofilm formation: a clinically relevant microbiological process. *Clin*  
548 *Infect Dis.* 33(8):1387-1392.

549 Donlan RM. 2002. Biofilms: microbial life on surfaces. *Emerg Infect Dis.* 8(9):881-890.

550 Dorel C, Lejeune P, Jubelin G. 2006. Role of biofilms in infections caused by *Escherichia*  
551 *coli*. In: Pace JL, Rupp ME, Finch R, editors. Biofilms, infection, and antimicrobial  
552 therapy. Boca Raton (USA): Taylor & Francis; p. 73-80.

553 Duetz WA. 2007. Microtiter plates as mini-bioreactors: miniaturization of fermentation  
554 methods. Trends Microbiol. 15(10):469-475.

555 Duetz WA, Ruedi L, Hermann R, O'Connor K, Buchs J, Witholt B. 2000. Methods for  
556 intense aeration, growth, storage, and replication of bacterial strains in microtiter plates.  
557 Appl Environ Microbiol. 66(6):2641-2646.

558 Dunne WM, Jr. 2002. Bacterial Adhesion: Seen Any Good Biofilms Lately? Bacterial  
559 Adhesion: Seen Any Good Biofilms Lately? 15(2):155-166.

560 Foxman B. 2002. Epidemiology of urinary tract infections: incidence, morbidity, and  
561 economic costs. Dis Mon. 49(2):53-70.

562 Frias J, Ribas F, Lucena F. 2001. Effects of different nutrients on bacterial growth in a  
563 pilot distribution system. Antonie Van Leeuwenhoek. 80(2):129-138.

564 Fux CA, Wilson S, Stoodley P. 2004. Detachment characteristics and oxacillin resistance  
565 of *Staphylococcus aureus* biofilm emboli in an in vitro catheter infection model. J  
566 Bacteriol. 186(14):4486-4491.

567 Ganderton L, Chawla J, Winters C, Wimpenny J, Stickler D. 1992. Scanning electron  
568 microscopy of bacterial biofilms on indwelling bladder catheters. Eur J Clin Microbiol  
569 Infect Dis. 11(9):789-796.

570 Hancock V, Ferrières L, Klemm P. 2007. Biofilm formation by asymptomatic and  
571 virulent urinary tract infectious *Escherichia coli* strains. FEMS Microbiol Lett.  
572 267(1):30-37.

573 Hermann R, Lehmann M, Büchs J. 2003. Characterization of gas-liquid mass transfer  
574 phenomena in microtiter plates. Biotechnol Bioeng. 81(2):178-186.

575 Hirt CW, Nichols BD. 1981. Volume of fluid (VOF) method for the dynamics of free  
576 boundaries. *J Comput Phys.* 39(1):201-225.

577 Holubar P, Andorfer C, Braun R. 1999. Effects of nitrogen limitation on biofilm  
578 formation in a hydrocarbon-degrading trickle-bed filter. *Appl Microbiol Biotechnol.*  
579 51(4):536-540.

580 Huang C-T, Peretti SW, Bryers JD. 1994. Effects of medium carbon-to-nitrogen ratio on  
581 biofilm formation and plasmid stability. *Biotechnol Bioeng.* 44(3):329-336.

582 Inauen W, Baumgartner H, Bombeli T, Haeberli A, Straub P. 1990. Dose- and shear rate-  
583 dependent effects of heparin on thrombogenesis induced by rabbit aorta subendothelium  
584 exposed to flowing human blood. *Arterioscler Thromb Vasc Biol.* 10(4):607-615.

585 Jacobsen SM, Stickler DJ, Mobley HLT, Shirtliff ME. 2008. Complicated catheter-  
586 associated urinary tract infections due to *Escherichia coli* and *Proteus mirabilis*. *Clin*  
587 *Microbiol Rev.* 21(1):26-59.

588 Kensy F, Zimmermann HF, Knabben I, Anderlei T, Trauthwein H, Dingerdissen U,  
589 Büchs J. 2005. Oxygen transfer phenomena in 48-well microtiter plates: determination  
590 by optical monitoring of sulfite oxidation and verification by real-time measurement  
591 during microbial growth. *Biotechnol Bioeng.* 89(6):698-708.

592 Klahre J, Flemming HC. 2000. Monitoring of biofouling in papermill process waters.  
593 *Water Res.* 34(14):3657-3665.

594 Kostenko V, Salek MM, Sattari P, Martinuzzi RJ. 2010. *Staphylococcus aureus* biofilm  
595 formation and tolerance to antibiotics in response to oscillatory shear stresses of  
596 physiological levels. *FEMS Immunol Med Microbiol.* 59(3):421-431.

597 Leroy C, Delbarre C, Ghillebaert F, Compere C, Combes D. 2007. Effects of commercial  
598 enzymes on the adhesion of a marine biofilm-forming bacterium. *Biofouling.* 24(1):11-  
599 22.



600 Liu Y, Tay J-H. 2002. The essential role of hydrodynamic shear force in the formation of  
601 biofilm and granular sludge. *Water Res.* 36(7):1653-1665.

602 Mareels G. 2007. Experimental and numerical modeling of flow and mass transport in a  
603 bioartificial liver [PhD]. Ghent (BE): Ghent University.

604 Mareels G, Kaminsky R, Eloot S, Verdonck PR. 2007. Particle image velocimetry-  
605 validated, computational fluid dynamics-based design to reduce shear stress and  
606 residence time in central venous hemodialysis catheters. *ASAIO J.* 53(4):438-446

607 McClaine JW, Ford RM. 2002. Characterizing the adhesion of motile and nonmotile  
608 *Escherichia coli* to a glass surface using a parallel-plate flow chamber. *Biotechnol*  
609 *Bioeng.* 78(2):179-189.

610 Michelson AD. 2002. Platelets. New York (USA): Academic Press/Elsevier Science.

611 Moreira JMR, Teodósio JS, Silva FC, Simões M, Melo LF, Mergulhão FJ. 2013a.  
612 Influence of flow rate variation on the development of *Escherichia coli* biofilms.  
613 *Bioprocess Biosyst Eng.* 1-10.

614 Moreira JMR, Gomes LC, Araújo JDP, Miranda JM, Simões M, Melo LF, Mergulhão FJ.  
615 2013b. The effect of glucose concentration and shaking conditions on *Escherichia coli*  
616 biofilm formation in microtiter plates. *Chem Eng Sci.* 94(0):192-199.

617 Mukherjee PK, Chand DV, Chandra J, Anderson JM, Ghannoum MA. 2009. Shear stress  
618 modulates the thickness and architecture of *Candida albicans* biofilms in a phase-  
619 dependent manner. *Mycoses.* 52(5):440-446.

620 Newman DK. 2008. Internal and external urinary catheters: a primer for clinical practice.  
621 *Ostomy Wound Manag.* 54(12):18-35.

622 Ortiz-Ochoa K, Doig SD, Ward JM, Baganz F. 2005. A novel method for the  
623 measurement of oxygen mass transfer rates in small-scale vessels. *Biochem Eng J.*  
624 25(1):63-68.

625 Percival SL, Knapp JS, Wales DS, Edyvean RGJ. 1999. The effect of turbulent flow and  
626 surface roughness on biofilm formation in drinking water. *J Ind Microbiol Biot.*  
627 22(3):152-159.

628 Pereira MO, Vieira MJ. 2001. Effects of the interactions between glutaraldehyde and the  
629 polymeric matrix on the efficacy of the biocide against *Pseudomonas fluorescens*  
630 biofilms. *Biofouling.* 17(2):93-101.

631 Peyton BM. 1996. Effects of shear stress and substrate loading rate on *Pseudomonas*  
632 *aeruginosa* biofilm thickness and density. *Water Res.* 30(1):29-36.

633 Rochex A, Lebeault JM. 2007. Effects of nutrients on biofilm formation and detachment  
634 of a *Pseudomonas putida* strain isolated from a paper machine. *Water Res.* 41(13):2885-  
635 2892.

636 Rodrigues DF, Elimelech M. 2009. Role of type 1 fimbriae and mannose in the  
637 development of *Escherichia coli* K12 biofilm: from initial cell adhesion to biofilm  
638 formation. *Biofouling.* 25(5):401-411.

639 Salek M, Sattari P, Martinuzzi R. 2012. Analysis of fluid flow and wall shear stress  
640 patterns inside partially filled agitated culture well plates. *Ann Biomed Eng.* 40(3):707-  
641 728.

642 Salo J, Sevander JJ, Tapiainen T, Ikaheimo I, Pokka T, Koskela M, Uhari M. 2009.  
643 Biofilm formation by *Escherichia coli* isolated from patients with urinary tract infections.  
644 *Clin Nephrol.* 71(5):501-507.

645 Schinabeck MK, Ghannoum MA. 2006. Biofilm-related indwelling medical device  
646 infections. In: Pace JL, Rupp ME, editors. *Biofilms, infection, and antimicrobial therapy.*  
647 Boca Raton (USA): Taylor & Francis; p. 39-48.

648 Shakeri S, Kermanshahi RK, Moghaddam MM, Emtiazi G. 2007. Assessment of biofilm  
649 cell removal and killing and biocide efficacy using the microtiter plate test. *Biofouling*.  
650 23(2):79-86.

651 Simões L, Simões M, Vieira M. 2010a. Adhesion and biofilm formation on polystyrene  
652 by drinking water-isolated bacteria. *Antonie van Leeuwenhoek*. 98(3):317-329.

653 Simões M, Pereira MO, Vieira MJ. 2005. Validation of respirometry as a short-term  
654 method to assess the efficacy of biocides. *Biofouling*. 21(1):9-17.

655 Simões M, Simões LC, Vieira MJ. 2010b. A review of current and emergent biofilm  
656 control strategies. *LWT-Food Sci Technol*. 43(4):573-583.

657 Simões M, Pereira MO, Sillankorva S, Azeredo J, Vieira MJ. 2007. The effect of  
658 hydrodynamic conditions on the phenotype of *Pseudomonas fluorescens* biofilms.  
659 *Biofouling*. 23(4):249-258.

660 Singh PK, Marzo A, Howard B, Rufenacht DA, Bijlenga P, Frangi AF, Lawford PV,  
661 Coley SC, Hose DR, Patel UJ. 2010. Effects of smoking and hypertension on wall shear  
662 stress and oscillatory shear index at the site of intracranial aneurysm formation. *Clin*  
663 *Neurol Neurosurg*. 112(4):306-313.

664 Sonak S, Bhosle NB. 1995. A simple method to assess bacterial attachment to surfaces.  
665 *Biofouling*. 9(1):31-38.

666 Stoodley P, Dodds I, Boyle JD, Lappin-Scott HM. 1998. Influence of hydrodynamics and  
667 nutrients on biofilm structure. *J Appl Microbiol*. 85(S1):19S-28S.

668 Stoodley P, Wilson S, Hall-Stoodley L, Boyle JD, Lappin-Scott HM, Costerton JW. 2001.  
669 Growth and detachment of cell clusters from mature mixed-species biofilms. *Appl*  
670 *Environ Microbiol*. 67(12):5608-5613.

671 Telgmann U, Horn H, Morgenroth E. 2004. Influence of growth history on sloughing and  
672 erosion from biofilms. *Water Res*. 38(17):3671-3684.

673 Teodósio JS, Simões M, Mergulhão FJ. 2012. The influence of nonconjugative  
674 *Escherichia coli* plasmids on biofilm formation and resistance. J Appl Microbiol 113:373-  
675 382.

676 Teodósio JS, Simões M, Melo LF, Mergulhão FJ. 2011a. The influence of the nutrient  
677 load on the formation of *Escherichia coli* biofilms. In: Berhardt LV, editors. Advances in  
678 Medicine and Biology. New York (USA): Nova Science Publishers, Inc.; p. 153-168.

679 Teodósio JS, Simões M, Melo LF, Mergulhão FJ. 2011b. Flow cell hydrodynamics and  
680 their effects on *E. coli* biofilm formation under different nutrient conditions and turbulent  
681 flow. Biofouling. 27(1):1-11.

682 Teodósio JS, Silva FC, Moreira JMR, Simões M, Melo LF, Alves MA, Mergulhão FJ.  
683 2013. Flow cells as quasi ideal systems for biofouling simulation of industrial piping  
684 systems. Biofouling.1-14.

685 Thomas WE, Trintchina E, Forero M, Vogel V, Sokurenko EV. 2002. Bacterial adhesion  
686 to target cells enhanced by shear force. Cell. 109(7):913-923.

687 Tran V, Fleiszig S, Evans D, Radke C. 2011. Dynamics of flagellum- and pilus-mediated  
688 association of *Pseudomonas aeruginosa* with contact lens surfaces. Appl Environ  
689 Microbiol. 77(11):3644-3652.

690 Tranoudis I, Efron N. 2004. Tensile properties of soft contact lens materials. Cont Lens  
691 Anterior Eye. 27(4):177-191.

692 Ulett GC, Mabbett AN, Fung KC, Webb RI, Schembri MA. 2007. The role of F9 fimbriae  
693 of uropathogenic *Escherichia coli* in biofilm formation. Microbiology. 153(7):2321-  
694 2331.

695 van Loosdrecht MCM, Eikelboom D, Gjaltema A, Mulder A, Tjihuis L, Heijnen JJ. 1995.  
696 Biofilm structures. Water Sci Technol. 32(8):35-43.

697 Vejborg RM, Klemm P. 2008. Blocking of bacterial biofilm formation by a fish protein  
698 coating. *Appl Environ Microbiol.* 74(11):3551-3558.

699 Velraeds M, van de Belt-Gritter B, Van der Mei H, Reid G, Busscher H. 1998. Interface  
700 in initial adhesion of uropathogenic bacteria and yeasts to silicone rubber by a  
701 *Lactobacillus acidophilus* biosurfactant. *J Med Microbiol.* 47:1081-1085.

702 Vieira MJ, Melo LF, Pinheiro MM. 1993. Biofilm formation: hydrodynamic effects on  
703 internal diffusion and structure. *Biofouling.* 7(1):67-80.

704 Volk CJ, LeChevallier MW. 1999. Impacts of the reduction of nutrient levels on bacterial  
705 water quality in distribution systems. *Appl Environ Microbiol.* 65(11):4957-4966.

706 Wäsche S, Horn H, Hempel DC. 2002. Influence of growth conditions on biofilm  
707 development and mass transfer at the bulk/biofilm interface. *Water Res.* 36(19):4775-  
708 4784.

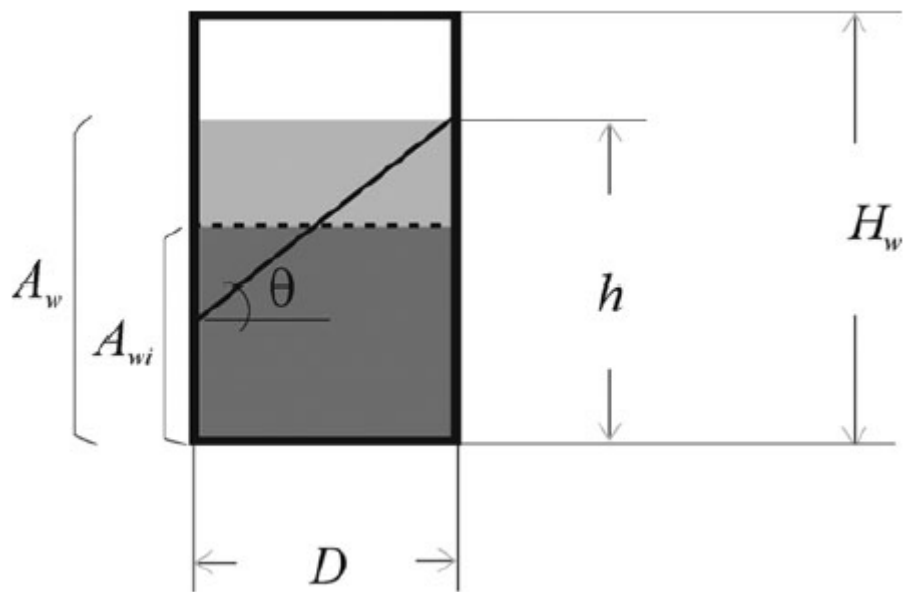
709 Weinstein RA, Darouiche RO. 2001. Device-associated infections: a macroproblem that  
710 starts with microadherence. *Clin Infect Dis.* 33(9):1567-1572.

711 Yataghene M, Pruvost J, Fayolle F, Legrand J. 2008. CFD analysis of the flow pattern  
712 and local shear rate in a scraped surface heat exchanger. *Chem Eng Process.* 47(9-  
713 10):1550-1561.

714 Youngs DL. 1982. Time-dependent multi-material flow with large fluid distortion. In:  
715 Morton KW, Baibnes MJ, editors. *Numerical methods for fluid dynamics.* New York  
716 (USA): Academic Press; p. 273-285.

717 Zhang H, Lamping SR, Pickering SCR, Lye GJ, Shamlou PA. 2008. Engineering  
718 characterisation of a single well from 24-well and 96-well microtitre plates. *Biochem Eng*  
719 *J.* 40(1):138-149.

720



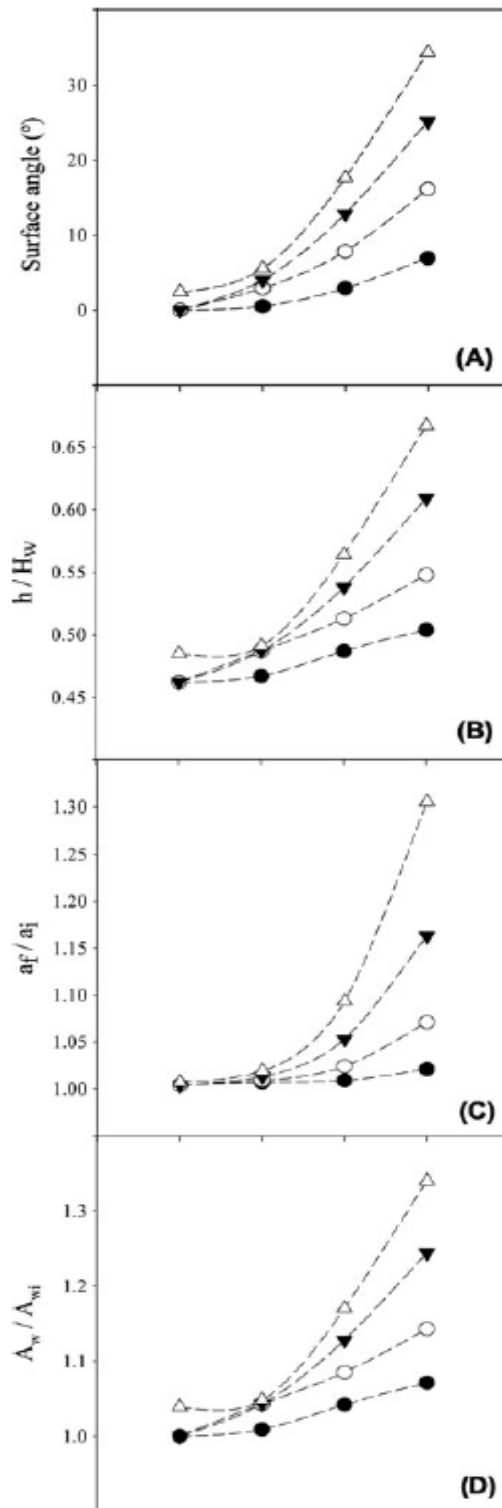
721

722 Figure 1. Schematic representation of a well. Dark grey area represents the wetted area in

723 a stationary well ( $A_{wi}$ ) and light grey area represents the area increase upon shaking ( $A_w$ ).

724  $D$  is the well diameter,  $h$  is the maximum height of the interface,  $H$  is the well height and

725  $\theta$  is the surface angle.



726

727 Figure 2. Simulation results of the effect of shaking frequency and amplitude on the (A)  
 728 surface angle, (B) maximum height of the interface ( $h$ ) normalized by the well height ( $H$ ),  
 729 (C) specific air-liquid surface area ( $a_f/a_i$ ), (D) ratio between the wetted area for a  
 730 dynamic ( $A_w$ ) and a stationary well ( $A_{wi}$ ). Open triangles ( $\Delta$ ) - 100 mm shaking  
 731 diameter, closed inverted triangle ( $\blacktriangledown$ ) - 75 mm shaking diameter, open circles ( $\circ$ ) - 50  
 732 mm shaking diameter, closed black circle ( $\bullet$ ) - 25 mm shaking diameter.

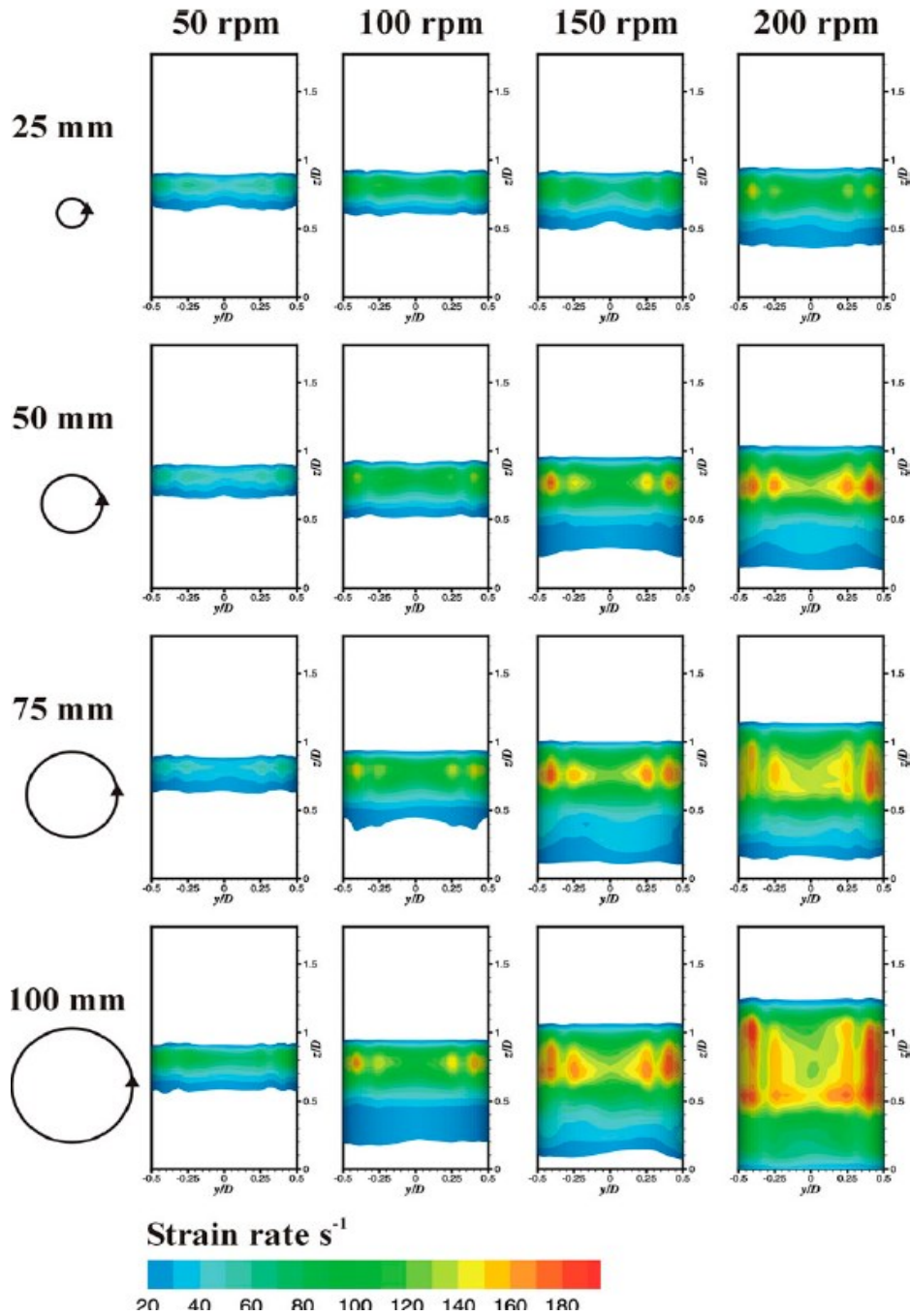
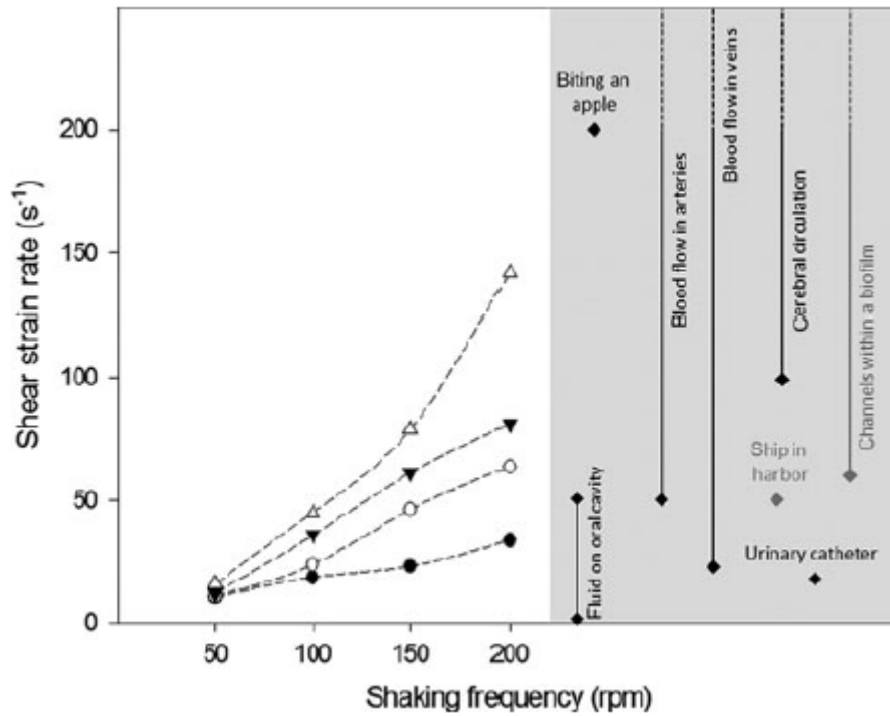


Figure 3. Time averaged strain rates on a 96-well microtiter plate at different orbital shaking diameters and shaking frequencies. The diameter of the circle is proportional to the diameter of the orbit described by each well of the plate when placed on an orbital incubator with the indicated orbital shaking diameter. Strain rates below  $20 \text{ s}^{-1}$  are not represented.

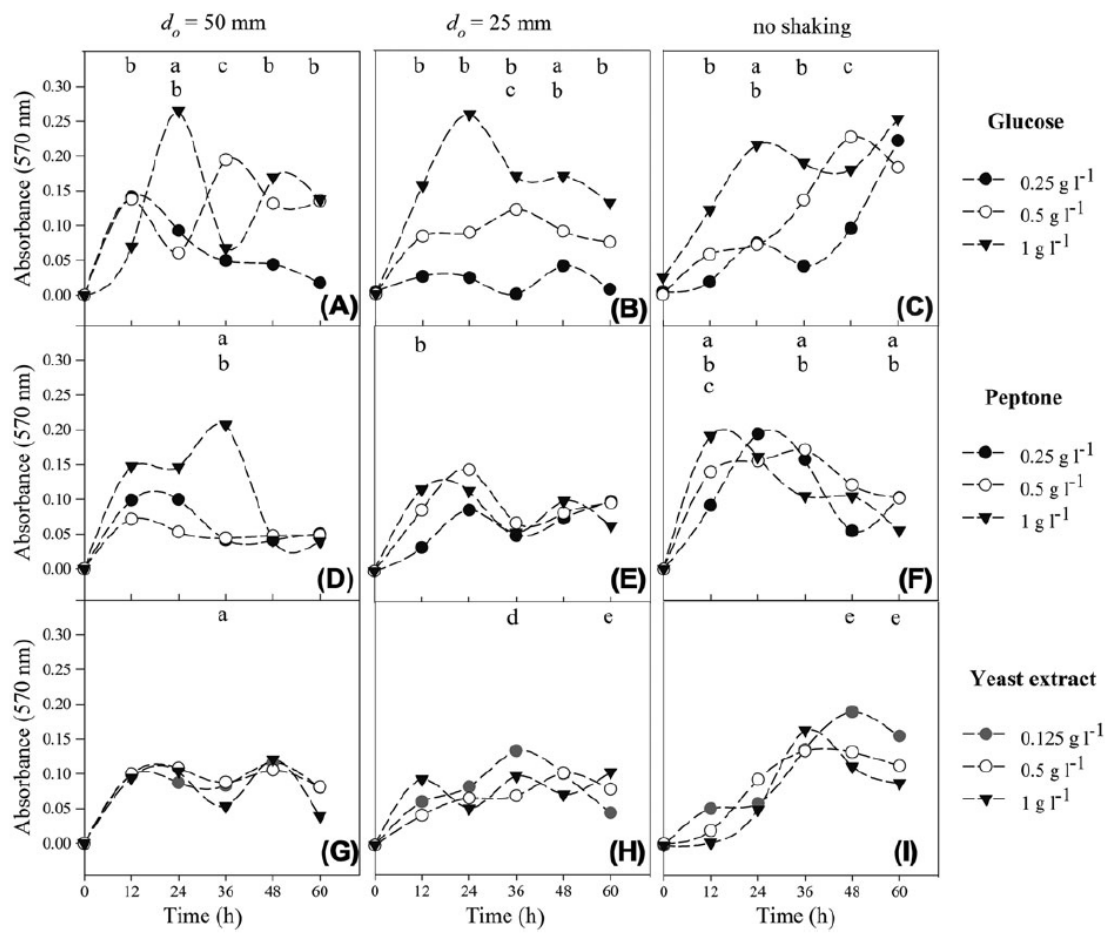




740

741 Figure 4. Numerical results of the shear strain rate as a function of the shaking frequency  
 742 for different orbital shaking diameters: open triangles ( $\Delta$ ) - 100 mm, closed inverted  
 743 triangle ( $\nabla$ ) - 75 mm, open circles ( $\circ$ ) - 50 mm, closed black circle ( $\bullet$ ) - 25 mm. The  
 744 grey shading include some shear rates found in biomedical ( $\blacklozenge$ ) and other scenarios ( $\blacklozenge$ )  
 745 (references on Table 1).

746



747

748 Figure 5. *E. coli* biofilm formation (absorbance at 570 nm) in 96-well microtiter plates  
 749 under dynamic ( $d_o = 50$  mm or 25 mm, 150 rpm) and static conditions: (A), (B) and (C)  
 750 effect of glucose; (D), (E) and (F) effect of peptone; (G), (H) and (I) effect of yeast extract.  
 751 Three nutrient concentrations were tested: closed inverted triangle ( $\blacktriangledown$ ) -  $1 \text{ g l}^{-1}$  of glucose,  
 752 peptone and yeast extract; open circle ( $\circ$ ) -  $0.5 \text{ g l}^{-1}$  of glucose, peptone and yeast extract;  
 753 closed black circle ( $\bullet$ ) -  $0.25 \text{ g l}^{-1}$  of glucose and peptone; closed gray circle ( $\bullet$ ) -  $0.125$   
 754  $\text{ g l}^{-1}$  of yeast extract. Results are an average of three independent experiments for each  
 755 condition. Average SDs were  $< 30\%$  for 50 mm shaking diameter,  $< 24\%$  for 25 mm  
 756 shaking diameter and  $< 25\%$  for no shaking conditions. Statistical analysis corresponding  
 757 to each time point is represented for a confidence level greater than 95% ( $P < 0.05$ ): a -  
 758 comparison between  $1 \text{ g l}^{-1}$  and  $0.5 \text{ g l}^{-1}$  glucose or peptone or yeast extract, b - comparison  
 759 between  $1 \text{ g l}^{-1}$  and  $0.25 \text{ g l}^{-1}$  glucose or peptone, c - comparison between  $0.5 \text{ g l}^{-1}$  and  
 760  $0.25 \text{ g l}^{-1}$  glucose or peptone, d - comparison between  $0.5 \text{ g l}^{-1}$  and  $0.125 \text{ g l}^{-1}$  yeast extract,  
 761 e - comparison between  $1 \text{ g l}^{-1}$  and  $0.125 \text{ g l}^{-1}$  yeast extract.

762

763 Table 1. Characteristic shear strain rates found in biomedical and other settings

	<b>Phenomenon</b>	<b>Shear strain rate (s<sup>-1</sup>)</b>	<b>Reference</b>
<b>Eyes</b>	Blinking of an eye	0.35	(Bakker et al. 2003, Tranoudis & Efron 2004)
	On-eye contact lens motion	1,000	(Tran et al. 2011)
<b>Mouth</b>	Fluid on oral cavity	0.1-50	
	On teeth, while biting an apple	200	(Bakker et al. 2003)
<b>Urinary tract</b>	Urinary flow in a catheter	15	(Bakker et al. 2003, Velraeds et al. 1998)
<b>Cardiovascular System</b>	Blood flow in veins	20-800	(Aleviadrou & McIntire 1995, Inauen et al. 1990, Michelson 2002)
	Blood flow in arteries	50-650	(Aleviadrou & McIntire 1995, Bark et al. 2012, Michelson 2002)
	Central venous hemodialysis catheters	1,900-2,400	(Mareels et al. 2007)
	Blood flow in little blood vessels	2,000-5,000	(Aleviadrou & McIntire 1995, Mareels 2007)
<b>Brain</b>	Cerebral circulation	> 100	(Singh et al. 2010)
<b>Other</b>	Flow of a film over a vertical plate	0.1	(Bakker et al. 2003)
	Annular space of a scraped surface heat exchanger	< 40	(Yataghene et al. 2008)
	Tumbling or pouring	10-100	(Bakker et al. 2003)
	Wall of a planetary mixer during cake batters	20-500	(Chesterton et al. 2011)
	Ship in harbor	50	
	Channels within a biofilm	60-300	(Bakker et al. 2003)

764  
765